ACS OMEGA

http://pubs.acs.org/journal/acsodf

Article

Spray Mode and Monodisperse Droplet Properties of an Electrospray

Ji Yeop Kim, Sang Ji Lee, and Jung Goo Hong*

Cite This: *ACS Omega* 2022, 7, 28667−28674

Read Online

ACCESS | Metrics & More | Article Recommendations

ABSTRACT: As a method of fluid atomization via application of a high voltage, electrospraying forms more uniform droplets than other spraying modes. This approach involves various spraying modes depending on the applied voltage. Most previous studies on electrospraying focused on the cone jet mode, which has limited applications since the applied voltage has a narrow range. To overcome this limitation, it is necessary to consider alternative spray modes, which require an in-depth understanding of their characteristics. To compare different spray modes, an investigation was conducted based on experimental parameters and fluid properties. In this study, a total of nine modes were identified, and the droplet characteristics in four modes were compared. The maximum deviation of the Sauter mean diameter (SMD) between the spray modes was approximately 1.7 times, and the SMD standard deviation was up to 2.8 times. In addition, the conditions required to realize Coulomb fission and monodisperse distribution depending on the Rayleigh critical charge (RSD < 6.76) were compared and examined.

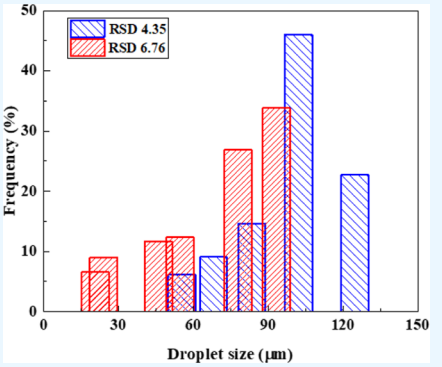

1. INTRODUCTION

Electrospraying is a method of fluid atomization by applying a high voltage using an auxiliary device, which results in the generation of uniform and continuous droplets.[1] Since the electrospray system requires the use of electrical signals, it can achieve faster responses and excellent reproducibility compared to other spray systems.[2] In the electrospray system, the droplet size and movement can be easily controlled by changing the external environment, and its structure is simpler than that of other spray systems since it can be configured by adjusting the applied high voltage.[3,4] In addition, repulsion between droplets occurs because they are sprayed into the electric field between the nozzle and a substrate, and the droplets are charged with (−) ions on their surface.[5] As a result, polymerization and combination rarely occur between different droplets.[6] Therefore, it is possible to generate uniform and fine droplets compared to other spray systems, and scattering is minimal owing to the characteristics of the charged droplets.[7−10] Based on these characteristics, electrospraying has been applied in various industrial fields, such as secondary battery electrolytes, surface coating spraying of ships, filter dust collectors to remove particulate matter, and food packaging manufacturing.[11−14]

Electrospraying facilitates diverse spraying modes depending on several physical variables and the fluid properties compared to typical pressure spraying. The spraying modes are divided into dripping, cone jet, and multijet. By varying the experimental parameters and fluid properties, the modes can be further divided into 14 modes, including microdripping, spindle, pulsed jet, rotating jet, ramified jet, tilted jet, and unstable.[15−17] The physical fluid property variables that significantly affect the formation and development of an electrospray mode are the fluid density, electrical conductivity, dielectric constant, viscosity, and surface tension. The experimental parameters include the distance between the nozzle and substrate, the nozzle diameter, flow rate, voltage, temperature, and humidity. These conditions have dominant effects on the different aspects of spray mode formation.[18,19]

Typical application fields depend on the electrospray mode. For example, microdripping is applied in patterning, oral drug devices, and inkjet printers.[20] The cone jet is used for paint spraying, uniform film fabrication, and local surface cooling,[21] whereas the pulsed jet is used in mass spectrometers, ion suppliers, etc.[22] Finally, the multijet is used in high-capacity particle generators and large-area film production.[23] Although electrospraying requires different fields depending on the mode since the range of each spray mode is limited according to the experimental parameters and physical properties, it is necessary to investigate the application of alternative modes with similar spray characteristics to improve performance.

Received: June 27, 2022
Accepted: July 26, 2022
Published: August 2, 2022

https://doi.org/10.1021/acsomega.2c04002
ACS Omega 2022, 7, 28667−28674

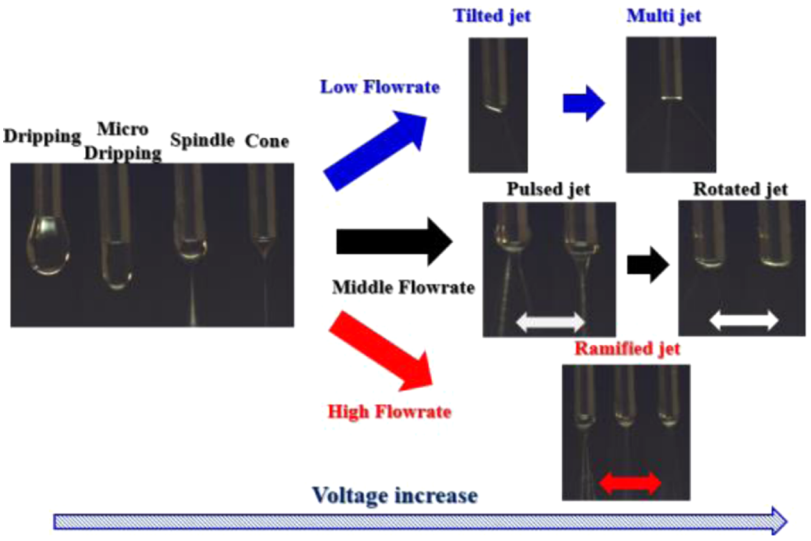

Figure 1. Electrospray images (photographs courtesy of Ji Yeop Kim. Copyright 2022).

Despite the various spray patterns and characteristics of electrospraying, most studies have focused on the cone jet.[24] This is because this spray pattern is relatively stable compared to other electrospraying modes, and facilitates a high water concentration and uniform particle generation with sizes ranging from several nm to tens of nm.[25−28] However, additional studies on the experimental parameters and fluid property factors of spray modes other than the cone jet are necessary since the spray mode depends on the fluid properties and experimental conditions, and certain spray modes are not realized during the process. Since the fluid properties and experimental conditions required to realize each spray mode are relatively narrow compared to other spray systems, studies should be conducted to gain an in-depth understanding of the modes and their applications, according to the average droplet size and distribution for each mode. Such studies can identify the spray characteristics of polymers with a high molecular weight under a low-flow rate condition, which is a disadvantage of electrospraying. Thus, studies on spray patterns according to different experimental parameters are important in terms of expanding the experimental conditions for electrospraying. In addition, since there are limited studies on the quantitative differences among electrospray modes, it is necessary to investigate the spray characteristics (droplet size and droplet distribution).

In previous electrospraying studies on the droplet size and distribution, the effect of fluid properties on the former was investigated. Ku et al.[29] determined that the average droplet size based on an empirical formula varied by up to four times compared to theoretical calculations. Sultan et al.[30] investigated only the droplet distribution and the size of the spindle, cone jet, and unstable modes using two-fluid and single-hole nozzles. Castillo-Orozco et al.[19] investigated the droplet size and distribution as a function of the applied voltage in microdripping. Le et al.[31] determined the droplet size and distribution according to the difference in the flow rate for the cone jet mode. Hollerbach et al.[32] examined the droplet size and distribution according to the applied voltage and physical properties. In these studies, the experimental conditions were limited, and most experiments were conducted in the range of the cone jet mode.

Therefore, in this study, the cone jet mode was compared to other modes to better understand the droplet characteristics as a function of fluid properties and physical variables. Instead of being limited to the cone jet mode, the flow experiment was performed for various spray modes to determine the applied voltage and the range of each mode, which were then compared to the cone jet mode. In addition, the purpose of this study was to examine the effects of several experimental variables for each mode based on the relationship between the Sauter mean diameter (SMD) and SMD standard deviation during spraying.

The main advantage of electrospraying is that it exhibits a monodisperse distribution compared to other spraying systems owing to the smaller flow rate and electrical loading. According to Jiang et al.,[33] when the charge on a droplet exceeds the critical charge in the cone jet mode using the Rayleigh critical charge, Coulomb fission, etc., a polydisperse distribution is observed. In this study, the relative standard deviation (RSD) of the cone jet mode was compared to that of other spray modes, and based on various experimental variables, an RSD value was obtained as a specific criterion for realizing a monodisperse distribution in the cone jet mode.

2. RESULTS AND DISCUSSION

2.1. Electrospray Mode Images. Figure 1 shows the different electrospraying modes for an increasing applied voltage and a varying flow rate. The dripping, microdripping, spindle, and cone modes were observed at all flow rates in the experiment, and these spray modes were formed in the given order as the applied voltage increased.[15] Although the dripping mode was not affected by the electric field, droplets were formed with a size of 1.80 times the nozzle diameter owing to the dominant influence of gravity. Droplets with a size similar to that of the nozzle diameter were deposited on a substrate. In microdripping, the droplet size was equal to or smaller than the nozzle diameter owing to the influence of the electric field, and in the case of the dripping mode, the formation of droplets occurred at a faster frequency.[16] In the spindle mode, a cone and jet were formed at the nozzle tip, which were broken up into droplets at a regular frequency. In addition, the cone was formed for a longer period, whereas the jet was wider compared to the cone jet mode during spraying. The cone

https://doi.org/10.1021/acsomega.2c04002
ACS Omega 2022, 7, 28667−28674

mode exhibited the most stable spray, and the length of the cone increased with an increasing applied voltage. Regardless of the length of the cone, a half spray angle of 49.3° was observed, as reported by Tang et al.[34] in a previous study. At a low flow rate (0.3 mL/h), a tilted jet or a multijet was formed as the applied voltage increased, following the formation of a stable cone shape. In the tilted jet, the jet at the tip of the cone was tilted to one side during spraying after the cone jet was formed. This occurred because of the influence of the electric field when the jet was broken up due to the surface shear stress from the tip of the cone. In the multijet, a weak cone was created and several jet branches developed simultaneously. Several jets were formed at a high applied voltage and flow rate. In addition, it was confirmed that a high flow rate increased the thickness of the jet, whereas a high applied voltage decreased the thickness. At an intermediate flow rate (1.5 mL/h), the pulsed and the rotated jets were formed as the applied voltage increased following the formation of a stable cone jet. In the pulsed jet, a cone and jet were formed, which could not be maintained owing to the occurrence of a periodic, and the droplets broke up directly from the nozzle. When the cone and jet were maintained, the cone was longer compared to that of a stable cone, whereas the jet was relatively thicker. In the rotating jet, the length of the cone was shorter than that of the stable cone, and the cone and jet were formed during clockwise rotation.

In the ramified jet under a high flow condition (6 mL/h), the spray pattern changed unstably compared to the stable cone jet, and a twin jet was generated at the tip of the thick cone during spraying. A simple jet spray mode was also observed, which is a characteristic of water. This is attributed to the combined influence of the high applied voltage and the flow rate.[16]

2.2. Spray Mode Sauter Mean Diameter (SMD) According to the Flow Rate. Figure 2 shows the Sauter mean diameter (SMD) and spray mode data depending on the applied voltage for flow rates of 0.3, 0.9, 1.5, and 6.0 mL/h using a solution, S. The experiment was conducted using a nozzle inner diameter of 1.0 mm and a nozzle-to-substrate distance of 25 mm. The SMD was the smallest in the cone jet at all flow rates. For a flow rate of 0.3 mL/h, the droplet size of the tilted jet was approximately 30% greater than that of the cone jet and that of the multijet was approximately 12% greater. At intermediate flow rates (0.9, 1.5 mL/h), the droplet size of the pulsed jet was 26% greater on average compared to that of the cone jet, whereas that of the rotating jet was approximately 15% smaller than that of the pulsed jet. Under a high flow condition (6.0 mL/h), the ramified jet and the rotated jet were generated by the applied voltage. The droplet sizes of the ramified and rotating jets were approximately 11 and 16% greater than that of the cone jet, respectively. As seen in the spray image in Figure 1, the length of the cone and the width of the jet formed in the spindle mode were relatively larger compared to those of the cone jet, possibly because the droplets were directly sprayed.[35]

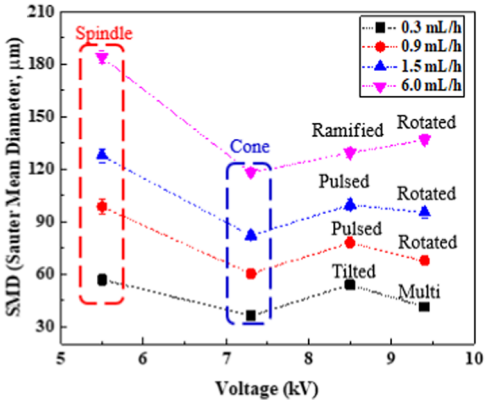

Figure 2. Sauter mean diameter (SMD) of spray mode according to the flow rate and applied voltage.

Figure 3 shows an SMD graph for the mixed solutions, S, V, and C, in the cone jet and spindle modes at various flow rates.

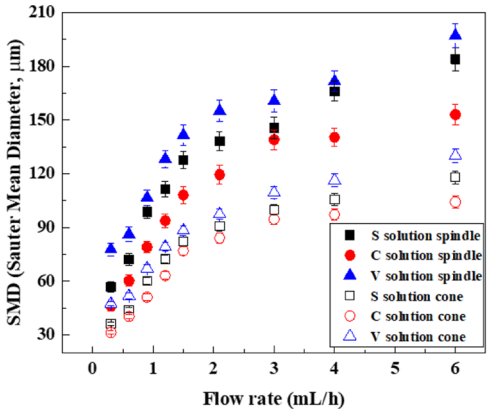

Figure 3. Solutions S, V, C, and SMD according to the flow rate in the cone jet and spindle modes.

The SMD increased linearly as the flow rate increased in both the spindle and cone jet modes. In addition, the difference in the SMD was similar among the spray modes depending on the mixed solution. The SMD at different flow rates gradually converged at a flow rate of 2.1 mL/h. This was attributed to the nozzle inner diameter of 1.0 mm, which prevented the SMD from increasing linearly as it gradually converged to the maximum flow rate. In both the spindle and cone jet modes, the SMD of solution V with a higher viscosity than that of solution S increased and the SMD of solution C with a higher electrical conductivity than that of solution S decreased. These phenomena can be explained by the increased fluid resistance in the case of solution V with high viscosity and by the tangential acceleration owing to the repulsion between (−) ions in the case of solution C with high electrical conductivity. In addition, the jet width of solution V was larger than that of solution S and the jet width of solution C was smaller than that of solution S.

Figure 4 shows the SMD data as a function of the spray mode at different flow rates. The SMD was found to increase in all spray modes as the flow rate increased, and the cone jet and spindle spray modes were realized under all flow conditions. The pulsed jet and rotated jet were observed at 0.9−3.0 and 1.5−6.0 mL/h, respectively. The SMD of the cone jet was the smallest for the changing flow rate and that of the spindle was the largest. Depending on the spray mode, the SMD of the rotated jet was 16% greater than that of the cone jet and that of the pulsed jet was approximately 23% greater. The SMD of the spindle was approximately 49% greater.

2.3. Spray Mode SMD Standard Deviation According to the Flow Rate. Figure 5 shows the Sauter mean diameter

https://doi.org/10.1021/acsomega.2c04002
ACS Omega 2022, 7, 28667−28674

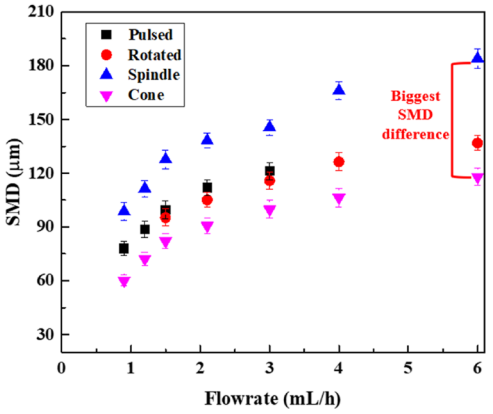

Figure 4. SMD difference according to the spray mode.

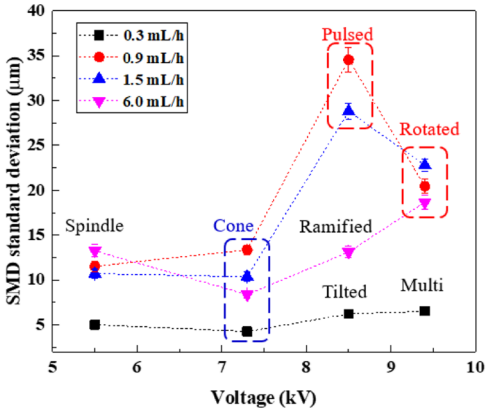

Figure 5. SMD standard deviation of the spray mode according to the flow rate and the applied voltage.

(SMD) and spray mode data as a function of the applied voltage and the flow rates of 0.3, 0.9, 1.5, and 6.0 mL/h using solution S. For the low-flow conditions, the SMD standard deviation was small and that of the cone jet was the smallest among the spray modes. In the case of the rotated jet and the pulsed jet, the standard deviation of the SMD based on the cone jet was relatively larger than that of the other spray modes. The flow experiments have shown that, relative to cone jets, the SMD deviation of the rotating jet is about 2 times higher and that of the pulse jet is about 2.7 times higher than that of the cone. It could be concluded that stable and uniform droplets were not generated in the rotating jet since the cone and jet rotate in the clockwise direction and the formation of the cone and jet in the pulsed jet was not stable owing to the pulse phenomenon, which caused the cone and jet to periodically break up into droplets. This resulted in a wide distribution of droplets.

Figure 6 shows the SMD standard deviation of the spray modes depending on the flow rate. Similar to the data in Figure 5, the SMD standard deviation of the rotating jet and the pulsed jet was larger than 2 times under all flow conditions and the SMD standard deviation of the pulsed jet was relatively larger than 30% of that of the rotating jet. In the case of the spindle, the SMD standard deviation was similar to that of the cone jet for all of the flow rates. Similar to the pulsed jet mode, a cone and jet were not formed in the spindle mode, but the frequency was smaller compared to that of the pulsed jet, and the SMD standard deviation was small since the spray pattern was similar to that of the cone jet.

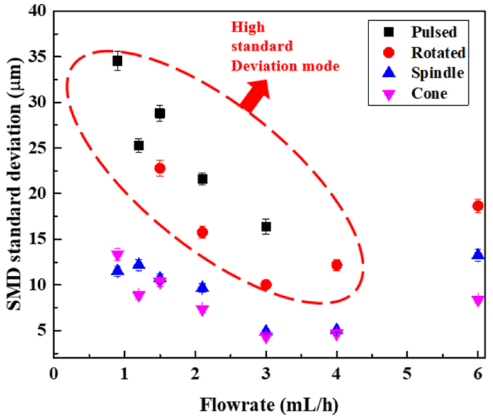

Figure 6. SMD standard deviation according to the flow rate for the different spray modes.

Figure 7 shows the size and frequency of the droplets in the cone jet, spindle, and pulse jet modes. The experiment was

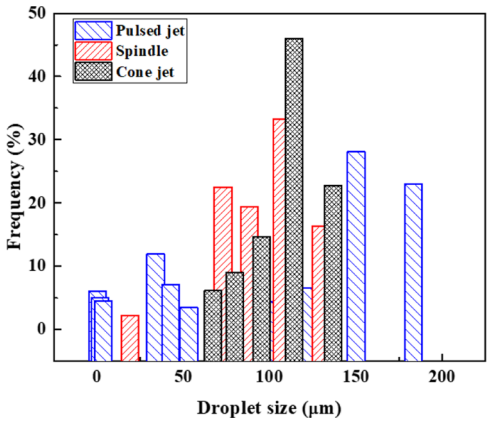

Figure 7. Droplet distribution according to the spray modes.

conducted using a nozzle-to-substrate distance of 25 mm, a nozzle inner diameter of 1.0 mm, and a flow rate of 3.0 mL/h. In the cone jet, droplets were formed with a size ranging from 60 to 130 μm, with a maximum frequency of 46% at 107 μm. In the spindle, droplets were formed with a size that ranged from 88 to 190 μm. with a maximum frequency of 33% at 107 μm. In the pulsed jet, the droplet size ranged from 7 to 190 μm. The pulsed jet had the widest range of droplets. The wide range of the droplet size in the pulsed jet was attributed to the occurrence of periodic pulses. The reason why pulse jet has a relatively wider droplet distribution compared to cone jets and spindle is that, in the case of pulse jets, pulsations are generated by an unstable spray pattern in the cone shape, and thus, droplet size ranges of three areas are formed. Although the droplet size in the spindle was larger than that in the cone jet, the SMD standard deviation, which was indicative of the advantageous size uniformity of electrospraying, was similar to that of the cone jet. In the case of the spindle, a shape similar to that of a cone jet was shown, and it was confirmed that large droplets were generated and the thickness of the cone was widened due to the shown unstable pattern. Therefore, it is expected that the spindle mode can be used instead of the cone jet mode under certain conditions.

2.4. Relative Standard Deviation (RSD) Data According to the Spray Mode. Table 1 shows the relative standard

https://doi.org/10.1021/acsomega.2c04002
ACS Omega 2022, 7, 28667−28674

Table 1. Relative Standard Deviation (RSD) Data

	cone jet	spindle	pulsed jet	rotated jet
flow rate (mL/h)	0.3−6.0	0.3−6.0	0.9−3.0	1.5−6.0
SMD (μm)	78.83	122.24	99.89	115.89
SMD standard deviation (μm)	7.54	8.93	25.32	15.89
RSD (%)	10.79	7.96	26.90	14.18

deviation (RSD) based on the data in Figure 7. The data in this table show the average value of each spray mode in the RSD according to the flow rate. The monodispersed distribution, one of the advantages of electrospraying, was examined according to the spray mode using the RSD to identify the characteristics of the monodisperse distribution. The formula for the RSD can be expressed as shown in eq 1.[36]

$$\frac{\text{SMD standard deviation}}{\text{SMD}} \times 100(\%) \quad (1)$$

The SMD and SMD standard deviation values were the smallest in the cone jet, whereas the RSD value was the smallest in the spindle mode with a large SMD. In addition, the SMD of the pulsed jet was similar to that of the cone jet, but the RSD was the largest owing to the large SMD standard deviation. Unlike a previous study by Jiang et al.,[33] who claimed that an RSD of 15% or less indicated a monodispersed distribution, the spindle mode exhibited a polydispersed distribution. The results of the previous study were determined to be different because the experiment was conducted only in the cone jet mode.

2.5. Rayleigh Limit According to the RSD. Figure 8 shows the data for the secondary breakup of droplets

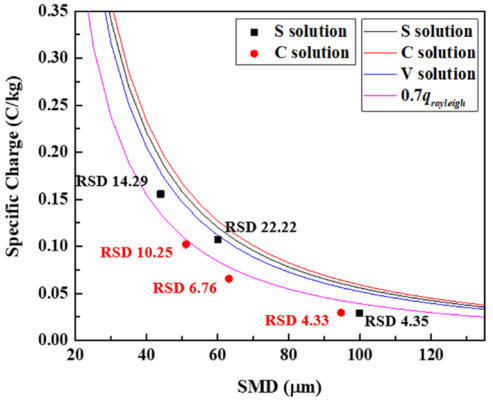

Figure 8. Rayleigh limit for solutions S and C according to the RSD.

depending on the RSD in the cone jet based on the data in Table 1. An RSD of 14.29% corresponds to solution S at 0.6 mL/h, an RSD of 22.22% corresponds to solution S at 0.9 mL/h, an RSD of 4.35% corresponds to solution S at 3.0 mL/h, an RSD of 10.25% corresponds to solution C at 0.9 mL/h, an RSD of 6.75% is associated with solution C at 1.2 mL/h, and an RSD of 4.33% corresponds to solution C at 3.0 mL/h. The charge value based on the SMD is expressed in eq 2.

$$\frac{q_{\text{Rayleigh}}}{m} = \frac{12\sqrt{2\varepsilon_0\sigma}}{\rho d^{3/2}} \quad (2)$$

Using eq 2, Jiang et al.[33] argued that a monodispersed distribution was observed when the Rayleigh value is 0.7 or smaller since secondary breakup did not occur, whereas secondary breakup occurred at a Rayleigh value greater than 0.7, resulting in a polydispersed distribution.

Figure 9 shows the SMD−frequency values for RSD values of 22.22, 14.29, and 10.25% with a Rayleigh value of 0.7 or

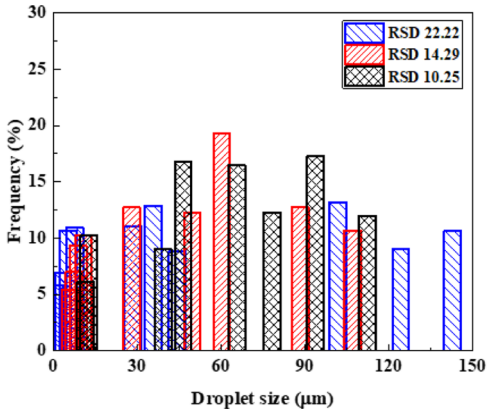

Figure 9. Bimodal graph according to the high RSD in the cone jet.

greater, at which a secondary breakup occurs. The droplet distribution exhibited a polydispersed distribution for all three RSDs, and the droplet size ranged from 6 to 148 μm. A polydispersed distribution was observed even at a smaller RSD value (10.25%) compared to that of the previous study that reported a polydispersed distribution at RSD < 15%. This result was attributed to the effects of the experimental conditions and fluid properties.

Figure 10 shows the SMD−Frequency values for RSD 4.35% and RSD 6.76% for a Rayleigh value below 0.7 at which

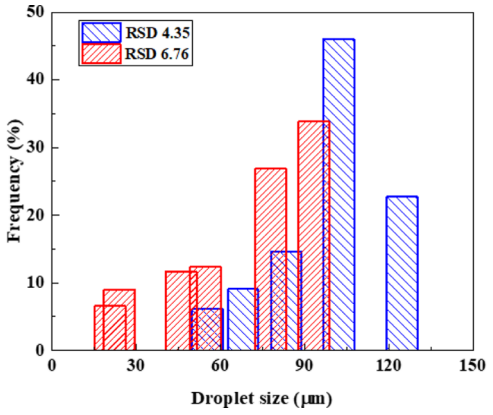

Figure 10. Monodisperse graph according to the low RSD in the cone jet.

secondary breakup does not occur. The droplet distribution exhibits a monodispersed distribution for both RSD values. In this experiment, a monodisperse distribution was observed for an RSD of 6.76% or less.

3. CONCLUSIONS

In an experimental study to investigate electrospraying characteristics as a function of the fluid properties and physical parameters, the droplet size and distribution were examined in terms of the SMD, SMD standard deviation, and the RSD for various spray modes, in addition to the effects on atomization.

https://doi.org/10.1021/acsomega.2c04002
ACS Omega 2022, 7, 28667−28674

1. Under the investigated electrostatic spraying conditions, the SMD was determined to increase as the flow rate and viscosity increased but decreased as the electrical conductivity increased.
2. Relative to the cone jet mode, the SMD was the largest in the spindle mode, whereas the SMD standard deviation was the largest in the rotating jet and pulsed jet modes.
3. The RSD was the smallest in the spindle mode, but the droplet distribution was the most uniform in the cone jet mode.
4. A monodisperse distribution was observed for an RSD of 6.76% or lower.

4. METHODS

4.1. Materials. In this experiment, the mixed solutions were prepared by adjusting the wt % using glycerol, ethanol, and citric acid. To prepare the solutions (glycerin, ethyl alcohol, and citric acid), glycerin (99%, Ducksan), ethyl alcohol (94%, Ducksan), and citric acid monohydrate (99.5%, Puriss, met the analytical specification of Ph. Eur., BP, USP, E330, Sigma-Aldrich) were used. Relative to solution S (ethanol 72 wt %, glycerol 18 wt %, and citric acid 10 wt %), solution C (ethanol 66.4 wt %, glycerol 13.3 wt %, and citric acid 20.3 wt %) had a higher conductivity and solution V (ethanol 55.3 wt %, glycerol 27.7 wt %, and citric acid 17 wt %) had a higher viscosity. The viscosities of the mixed solutions, S and V, varied by 2.3 times at 4.18 and 9.69 mPa·s, respectively, and the conductivities of the mixed solutions, S and C, varied by 1.72 times at 11.6 and 19.0 μs/cm, respectively. In addition to viscosity and conductivity, other physical properties including the surface tension (25.54−26.26 mN/m), dielectric constant (40.7−47.5), and density (940−1005 kg/m^3) were investigated.

4.2. Solution Stirring Method and Measurement of Properties. The mixed solution was prepared using a multiheating magnetic stirrer (S07-72-050, Mi-Sung). In this process, the ambient temperature was fixed at 25 °C. The solution was stirred for approximately 12 h at 60 rpm while sealed to prevent any external reaction. The electrical conductivity was measured using a EUTECH Portable Conductivity Meter CON-150, and the standard solution was corrected using 111.8 mS/cm. The viscosity was measured using an SV-10 kinematic viscometer, and the surface tension was measured using a dynamic contact angle and surface tension meter DCA-200. The dielectric constant was measured using a liquid dielectric constant meter 871.[35]

4.3. Experimental Setup. Figure 11 shows a diagram of the experimental setup. The center of the setup consisted of a fluid supply unit and an experimental parameter controller, which included a nozzle, a syringe pump, a cover, a substrate, and a support jack. A stainless steel nozzle with an inner diameter of 1.0 mm was used. A NE-1000 model was used as the syringe pump, and a 3cc syringe (HSW Norm-Ject) was used to supply the fluid. The cover was made of acrylic to minimize the influence of the external environment, and the rest was airtight. The substrate was prepared by directly processing to a height of 15 mm and a diameter of 50 mm using aluminum. In addition, a support jack was installed to adjust the height of the substrate. This experiment was conducted by fixing the distance between the nozzle and the substrate.

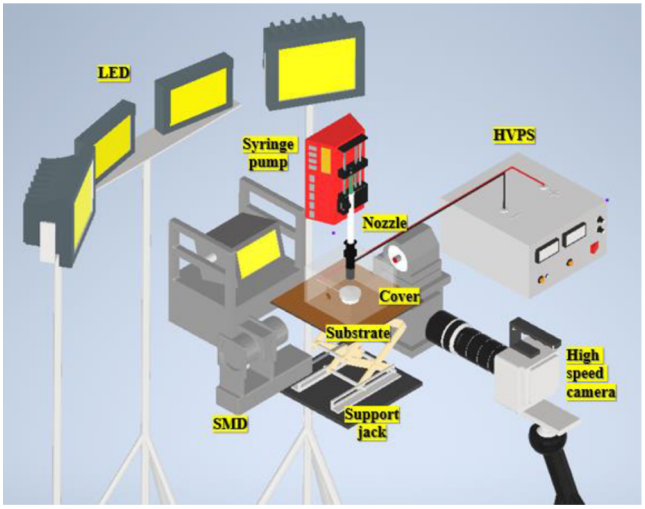

Figure 11. Schematic diagram of the experimental setup (photograph courtesy of Ji Yeop Kim. Copyright 2022).

Using the high-voltage supply unit on the right, a high voltage was applied using a power supply (HVPS; Korea Switching, C220, ∼30 kV, ∼15 mA), and the nozzle (−) and the substrate (+) were charged. In addition, an experiment was conducted by slowly increasing the applied voltage using an internal controller to minimize hysteresis.[37]

Spray visualization was confirmed using a high-speed camera (Phantom VEO E310L; maximum resolution, pixels 1200 × 800; sample rate, 11,500 f/s) and an light-emitting diode (LED) on the lower right and upper left. More than 500 spray images were analyzed under each experimental condition. The spray pattern images were captured after the spray mode reached a steady state for the applied voltage.[37] For lighting purposes, three backlights and two front incident lights were used to capture images of the subject. A total of five backlights and front incident lights were used since the former was useful for observing the details of the shape, and the latter allowed the outline of the spray mode to be more easily distinguishable. Since the frequency of lighting was 60 Hz, the frame value of the high-speed camera was set to at least 100 frames and the shutter speed was set to 1/9900 s. Continuous shooting was possible without interruption of the frames by maintaining a shutter speed of 60 Hz or higher. Since accurate values could not be obtained when shooting at a slower shutter speed, the aforementioned values can serve as a threshold. Since the focal distance was very short, the aperture was reduced to F11 to ensure an adequate depth of field for the subject.[35]

The SMD and SMD standard deviation were measured using Malvern's Spraytech (MLXA-A12-635-5) based on the line of sight principle.[38]

4.4. Experimental Conditions. The experiments were conducted at flow rates of 0.3, 0.6, 0.9, 1.2, 1.5, 1.8, 2.1, 3.0, 4.0, and 6.0 mL/h. The inner diameter of the nozzle was 1.0 mm, the distance between the nozzle and the substrate was 25 mm, and the atmospheric temperature was fixed at 25 °C to prevent changes to the fluid properties. The relative humidity, which could affect the spray pattern, droplet size, and droplet distribution, was set at 40 ± 10% for the experiment by installing a cover and adjusting the internal humidity.[35]

https://doi.org/10.1021/acsomega.2c04002
ACS Omega 2022, 7, 28667−28674

AUTHOR INFORMATION

Corresponding Author

Jung Goo Hong − *School of Mechanical Engineering, Kyungpook National University, Daegu 41566, Republic of Korea;* orcid.org/0000-0002-1286-5728; Phone: 82-53-950-6570; Email: jghong70@knu.ac.kr; Fax: 82-53-950-6550

Authors

Ji Yeop Kim − *School of Mechanical Engineering, Kyungpook National University, Daegu 41566, Republic of Korea*

Sang Ji Lee − *School of Mechanical Engineering, Kyungpook National University, Daegu 41566, Republic of Korea*

Complete contact information is available at: https://pubs.acs.org/10.1021/acsomega.2c04002

Notes

The authors declare no competing financial interest.

ACKNOWLEDGMENTS

This work was supported by the Human Resources Program in Energy Technology of the Korea Institute of Energy Technology Evaluation and Planning (KETEP), and financial resources were also provided by the Ministry of Trade, Industry & Energy, Republic of Korea (No. 20204010600060).

REFERENCES

(1) Lee, S. Y. *Atomization and Spray*; Minumsa: Korea, 1996; pp 155−164.

(2) Yuill, E. M.; Niya, S.; Steven, J. R.; Gary, M. H.; Lane, A. B. Electrospray Ionization from Nanopipette Emitters with Tip Diameters of Less than 100 nm. *Anal. Chem.* **2013**, *85*, 8498−8502.

(3) Chung, J. H.; Lee, H. B.; Kim, J. H. Electrohydrodynamic Assembly of Nanoparticles for Nanoengineered Biosensors. *Multiscale Simul. Mech. Biol. Mater.* **2013**, 193−206.

(4) Jayasinghe, S. N.; Townsend, N. A. Bio-electrosprays: the next generation of electrified jets. *Biotechnol. J.* **2006**, *1*, 1018−1022.

(5) Chen, L.; Chengbo, R.; Hongguo, Z.; Yanchun, Z.; Zhiwei, C.; Haoyuan, W.; Gang, L. Assembling Hybrid Energetic Materials with Controllable interfacial Microstructures by Electrospray. *ACS Omega* **2021**, *6*, 16816−16825.

(6) Liu, W. K.; Karpov, E. G.; Park, H. S. *Nano Mechanics and Materials: Theory, Multiscale Methods and Applications*, 1st ed.; John Wiley and Sons, 2006.

(7) Salata, O. V. Tools of Nanotechnolohy: Electrospray. *Curr. Nanosci.* **2005**, *1*, 25−33.

(8) Masr, G. G.; Yule, A. J.; Bending, L. *Industrial Sprays and Atomization: Design, Analysis and Applications*; Springer: London, 2002.

(9) Rietveld, I. B.; Kobayashi, K.; Yamada, H.; Matsushige, K. Electrospray deposition model, and experiment: Toward general-control of film morphology. *J. Phys. Chem. B* **2006**, *110*, 23351−23364.

(10) Basak, S.; Chen, D. R.; Biswas, P. Electrospray of ionic precursor solution to synthesize iron oxide nanoparticles:modified scalling law. *Chem. Eng. Sci.* **2007**, *62*, 1263−1268.

(11) Rahman, K.; Alli, K.; Muhammad, N. M.; Hyun, M. T.; Choi, K. H. Fine resolution drop-on-demand electrohydrodynamic patterning of conductive silver tracks on glass substrate. *Appl. Phys. A* **2013**, *111*, 593−600.

(12) Kim, J. W.; Duraisamy, N.; Lee, T. M.; Kim, I. K.; Choi, K. H. Hybrid electrohydrodynamic atomization of nanostructured silver top contact for inverted organic solar cells. *Sol. Energy Mater. Sol. Cells* **2014**, *130*, 156−162.

(13) Hogan, C. J., Jr.; Carroll, J. A.; Rohrs, H. W.; Biswas, P.; Gross, M. L. Combined Charged Residue-Field Emission Model of Macromolecular Electrospray Ionization. *Anal. Chem.* **2009**, *81*, 369−377.

(14) Chen, L.; Ru, C.; Zhang, H.; Zhang, Y.; Chi, Z.; Wang, H.; Li, G. Assembling Hybrid Energetic Materials with Controllable Interfacial Microstructures by Electrospray. *ACS Omega* **2021**, *6*, 16816−16825.

(15) Jaworek, A.; Krupa, A. Generation and characteristics of the precession mode of EHD spraying. *J. Aerosol Sci.* **1996**, *27*, 75−82.

(16) Laoonual, Y. Optical Investigation of Evaporating Spray. PhD Thesis, Imperial College London, 2006.

(17) Balgis, R.; Hiroyuki, M.; Takashi, O.; Makoto, K.; Li, B. Enhanced Aerosol Particle Filtration Efficiency of Nonwoven Porous Cellulose Triacetate Nanofiber Mats. *ACS Omega* **2018**, *3*, 8271−8277.

(18) Tang, L.; Kebarle, P. Effect of the conductivity of the electrosprayed solution on the electrospray current. Factors determing analyte sensitivity in electrospray mass spectrometry. *Anal. Chem.* **1991**, *63*, 2709−2715.

(19) Castillo-Orozco, E.; Aravinda, K.; Ranganathan, K. Nondimensional groups for electrospray modes of highly conductive and viscous nanoparticle suspensions. *Sci. Rep.* **2020**, *10*, No. 4405.

(20) Castillo-Orozco, E.; Aravinda, K.; Ranganathan, K. Electrospray mode transition of microdroplets with semiconductor nanoparticle suspension. *Sci. Rep.* **2017**, *7*, No. 5144.

(21) Rosell-Llompart, J.; Grifoll, J.; Loscetales, I. G. Electrosprays in the cone-jet mode: From Taylor cone formation to spray development. *J. Aerosol Sci.* **2018**, *125*, 2−31.

(22) Chong, E. S.; Hwang, G. B.; Kim, K. T.; Lee, I. S.; Han, S. H.; Kim, H. J.; Jung, H. H.; Kim, S. J.; Jung, H. I.; Lee, B. U. Viable Bacterial Cell Patterning Using a Pulsed Jet Electrospray System. *J. Microbiol. Biotechnol.* **2015**, *25*, 381−385.

(23) Ryan, C. N.; Smith, K. L.; Stark, J. P. W. Characterization of multi-jet electrospray systems. *J. Aerosol Sci.* **2012**, *51*, 35−48.

(24) Cloupeau, M.; Prunet-Foch, B. Electrohydrodynamic Spraying Functioning Modes: A Critical Review. *J. Aerosol Sci.* **1994**, *25*, 1021−1036.

(25) Gamero-Castano, M.; Hruby, V. Electrospray as a Source of Nanoparticles for Efficient Colloid Thrusters. *J. Propul. Power* **2001**, *17*, 977−987.

(26) Wu, Y.; Mackay, J. A.; McDaniel, J. R.; Chilkoti, A.; Clark, R. L. Fabrication of elastin like polypeptide nanoparticles for drung deliverly by electrospraying. *Biomacromolecules* **2008**, *10*, 19−24.

(27) Kim, H. C.; Kim, J. H.; Yang, H. J.; Suh, J. S.; Kim, T. Y.; Han, B. W.; Kim, S. W.; Kim, D. S.; Peter, V. P.; Choi, M. S. Parallel patterning of nanoparticles via electrodynamic focusing of charged aerosols. *Nat. Nanotechnol.* **2006**, *1*, 117−121.

(28) Wang, K.; Stark, J. P. Direct fabrication of electrically functional microstructures by fully voltage-controlled electrohydrodynamic jet printing of silver nonoink. *Appl. Phys. A* **2010**, *99*, 763−766.

(29) Ku, B. K.; Kim, S. S. Electrospray characteristics of highly viscous liquids. *J. Aerosol Sci.* **2002**, *33*, 1361−1378.

(30) Sultan, F.; Ashgriz, N.; Guildenbecher, D. R.; Sojka, P. E. *Handbook of Atomization and Sprays*, Ashgriz, N., Ed.; Springer: New York, 2011; pp 727−753.

(31) Le, N. T.; Myrick, J. M.; Seigle, T.; Huynh, P. T.; Krishnan, S. Mapping electrospray modes and droplet size distributions for chitosan solutions in unentangled and entangled concentration regimes. *Adv. Powder Technol.* **2018**, *29*, 3007−3021.

(32) Hollerbach, A.; Logsdon, D.; Iyer, K.; Li, A.; Schaberb, J. A.; Cooks, R. G. Sizing sub-diffraction limit electrosprayed droplets by structured illumination microscopy. *Analyst* **2018**, *143*, 232−240.

(33) Jiang, Z.; Gan, Y.; Ju, Y.; Liang, J.; Zhou, Y. Experimental study on the electrospray and combustion characteristics of biodiesel-ethanol blends in a meso-scale combustor. *Energy* **2019**, *179*, 843−849.

(34) Tang, K.; Gomez, A. Monodisperse Electrosprays of Low Electric Conductivity Liquids in the Cone-Jet Mode. *J. Colloid Interface Sci.* **1996**, *184*, 500−511.

(35) Kim, J. Y.; Lee, S. J.; Baik, G. Y.; Hong, J. G. Viscosity Effect on the Electrospray Characteristics of Droplet Size and Distribution. *ACS Omega* **2021**, *6*, 29724−29734.
(36) Schultz, G. A.; Corso, T. N.; Prosser, S. J.; Zhang, S. A Fully Integrated Monolithic Microchip Electrospray Device for Mass Spectrometry. *Anal. Chem.* **2000**, *72*, 4058−4063.
(37) Kim, J. Y.; Lee, S. J.; Baik, G. Y.; Hong, J. G. Effects of Working Fluids on Spray Modes and Atomization Characteristics in Electrospray. *J. Korean Soc. Precis. Eng.* **2021**, *38*, 61−68.
(38) Ku, K. W.; Hong, J. G.; Park, C. W. Effect of Assist-air of Twin Fluid Atomizer on Urea Thermal Decomposition. *Atomization Sprays* **2015**, *25*, 895−915.

https://doi.org/10.1021/acsomega.2c04002
ACS Omega 2022, 7, 28667−28674